Original Article

Studies on formability of sintered aluminum composites during hot deformation using strain hardening parameters

Sumesh Narayan*, Ananthanarayanan Rajeshkannan

Mechanical Engineering, School of Engineering and Physics, Faculty of Science, Technology & Environment, The University of the South Pacific, Suva, Fiji

ABSTRACT

Formability is the limit to which a material can be deformed before failure and is upmost importance in powder metallurgy (PM) forming process. This is because the presence of porosity in the PM part after the sintering process. In this study two key strain hardening parameters are used to study the workability behavior or determining the failure zone. This can be used for design of PM parts and most importantly the die design as repressing needs to be employed before pores appear as cracks on the free surface. It is nearly impossible to produce defect free parts if this failure occurs. The hot formability behavior of aluminum metal matrix composites (MMC's) that is, Al-4TiC, Al-4WC, Al-4Fe$_3$C and Al-4Mo$_2$C (by weight percentage) are presented in this paper.

1. Introduction

The forming limit of PM compacts is absolute important and the study of workability behavior of PM materials is an essential study in designing of the deformation process [1,2]. Workability of the PM compacts plays a key part to find out if the PM compact is shaped effectively or fracture starts during the deformation process. Workability is the amount of deformation and induced internal stresses a material can handle during upsetting prior to failure and depends on a number of deforming factors such as stress and strain rate, friction, temperature and material [3,4]. Several constitutive equations have been developed to appreciate the constitutive performance of PM parts during hot forming processes [5–7]. Further, formability stress factor (β) is proposed in [3] which describe the consequence of hydrostatic and equivalent stresses during the forming process. The authors have used the models developed earlier by Kuhn-Downey [8] and Whang-Kobayashi [9] and also studied the influence of density on formability behavior of PM parts during forming. During the forming process several fracture behavior is present that depends on the amount of triaxiality [10,11].

Shima and Oyane [12] and Green [13] studied workability (formability stress index and mean stress) and densification behavior looking at several round pores, axial stress and

---

initial theoretical density. Narayansamy et al. [14–16] presented the fracture mechanisms of PM parts in three different stress states, that is, plane, uniaxial and triaxial. Further, the authors have studied the technical relationship that exists between the hoop, mean and effective stresses against deformation and densification. Vujovic and Shabaik [17], Doraivelu et al. [18] and Ko et al. [19] suggested a novel forming limit measure for PM material confirming with experimentations and numerical works all based on formability stress index, hydrostatic and equivalent stress. The present investigation proposes to study the workability behavior by studying the strain hardening parameters, strain hardening exponent (ni) and stress coefficient (Ki). Several investigators studied strain hardening behavior to evaluate the densification and strain hardening behavior, however, hardly any research was conducted to find the forming limit using the two very important strain hardening parameters. The strain hardening coefficient and the stress coefficient are one of the basic forming constraints of metal matrix composites. Strain hardening studies are vital in the deformation process as it governs the extent of even plastic strain the metal can sustain throughout the deformation without failure.

Narayanasamy et al. [4] explored on the instant strain-hardening performance of a PM aluminum-iron alloy. The effect of various iron content and preform geometry on strain hardening and densification were established. Luo et al. [20] studied the influence of temperature, strain rate and strain on strain hardening. Further, a correlation between strain hardening parameters (ni and Ki) with axial strain and relative density was developed experimentally and used to evaluate the geometric and matrix work hardening [21,22]. An interesting point to note from these researches [20–22] is that during the initial stages the strain hardening increases rapidly and then decreases sharply. This behavior is due to large degree of deformation during the initial stages of deformation and needs to be neglected for all practical reasons. Then the strain hardening values maintain a steady behavior and finally during the last phase of forming there is fluctuation in the strain hardening values. This final stage can be analyzed to plot the forming limit diagram and determine the failure zone. The sintered forging process is widely used in industries for producing parts with uniform properties and complex geometry. Further, one of the quests today is producing high strength materials using green manufacturing such as PM manufacturing process.

The paper analyzes the formability limit of PM preforms of Al-4TiC, Al-4WC, Al-4Fe$_3$C and Al-4Mo$_2$C experimentally with the influence of preform geometry, initial relative density and various carbide reinforcements. The instantaneous strain hardening (ni) and instantaneous stress coefficient (Ki) is used to plot the forming limit diagram.

2. Materials and method

2.1. Materials

Nowadays, numerous investigators are working on producing frontier materials that will benefit our society in one way or another. Aluminum MMC's are in demand for industrial applications due to some very good properties, main one being high strength to density ratio [23,24]. Carbide reinforced aluminum are widely used as carbide particulate are good in wear and corrosion resistance, high strength and hardness. Hence, in this research work several aluminum MMC's are prepared using PM process and forming limit in investigated using the strain hardening parameters. Aluminum powder (150 μm in diameter) and carbide powders (50 μm in diameter) were used to prepare titanium carbide reinforced aluminum, tungsten carbide reinforced aluminum, molybdenum carbide reinforced aluminum and iron carbide reinforced aluminum composites for this study. The sieve analysis and basic characterization of aluminum powder and the corresponding composition was completed by standard procedures and given in Tables 1 and 2, respectively.

2.2. Experimental method

Required amount of powders were taken to prepare blends of the aforementioned compositions in a planetary ball mill, model Retsch PM400MA. The mixing process was conducted for 2 h at a speed of 200 rpm. The homogenous mixture was ensured by taking the apparent density and required intervals. The required amount of powders to produce Al-4TiC, Al-4WC, Al-4Fe$_3$C and Al-4Mo$_2$C with height-to diameter ratios (aspect ratio, AR) of 0.4 and 0.6 were compressed using a hydraulic press. The load was varied from 139 MPa to 159 MPa so that to achieve relative densities of 0.82 and 0.86. To prevent oxidation during the sintering process, these compacts were then covered with ceramic paste as described elsewhere [22] and were left for atmospheric drying for a period of 12 h and then at 220 °C for a period of 30 min in an electrical muffle furnace. Finally, the temperature was increased to 594 °C for the sintering process which further took 60 min.

Hot upsetting under dry friction condition was carried out at the sintering temperature to obtain various height strains until visible cracks can be seen on the free surface. Then all the compacts were left in atmospheric conditions to cool to room temperature after which dimensional measurements were taken to determine axial strain, effective strain, effective stress, hydrostatic stress, formability stress index, instantaneous stress coefficient and instantaneous strain hardening coefficient. Furthermore, Archimedes technique was used to determine the compact densities. The maximum deformed and undeformed specimens of each composition were cut into two halves and microstructural views were obtained at the diametrical end (near the edge).

2.3. Yield criteria

The following equation is used by many investigators [2,15]:

$$AJ_2^/ + BJ_1^2 = Y^2 = \delta Y_0^2 \tag{1}$$

Further, J_1 and $J_2^/$ in the cylindrical coordinate and for axisymmetric forging, $\sigma_r = \sigma_\theta$, is given by [15]

$$J_1^2 = 4\sigma_\theta^2 + \sigma_z^2 + 4\sigma_\theta\sigma_z \tag{2}$$

Table 1 – Sieve analysis of aluminum powder.						
Sieve size (µm)	250	+200	+150	+100	+75	+45	−45
Retention in sieve (weight %)	0.2	0.3	16.3	55.3	9.5	7.9	10.5

Table 2 – Characterization of aluminum powder and its blends.					
Property	Al	Al-4WC	Al-4TiC	Al-4Fe$_3$C	Al-4Mo$_2$C
Apparent density (g/cc)	1.091	1.345	1.186	1.308	1.325
Flow rate (s/50 g) by hall flow meter	87.306	79.647	85.202	80.559	80.481
Compressibility (g/cc) at pressure of 130 ± 10 MPa	2.356	2.113	2.280	2.235	2.210

$$J_2^{/} = \frac{1}{6}(2\sigma_\theta^2 + 2\sigma_z^2 - 4\sigma_\theta\sigma_z) \tag{3}$$

Substituting Eqs. (2) and (3) into Eq. (1) gives

$$\frac{A}{6}(2\sigma_\theta^2 + 2\sigma_z^2 - 4\sigma_\theta\sigma_z) + B(4\sigma_\theta^2 + \sigma_z^2 + 4\sigma_\theta\sigma_z) = \delta Y_0^2 \tag{4}$$

Doraivelu et al. [18], Shima and Oyane [12], Park [25], and Lee and Kim [26] studied the yield criterion parameters for Eq. (1) as presented in Table 3. It can be seen in Table 3 that Doraivelu et al. [18], Park [25] and Lee and Kim [26] have the same values for the yield criterion parameters, A and B, however, all have different values for yield criterion parameter, δ. To highlight the modifications, the values for δ is calculate for different relative density, R, of sintered PM parts, as given in Table 4. The range of R for PM materials is in the range of 0.80–1.0 for many industrial applications as well as for research. Hence, the initial density chosen for analysis in Table 4 is 0.80 and the R is varied in a range of 0.80–1.0 in increments of 0.04. It can be seen that when the R approaches 1, that is when the PM material is well compacted to approximately fully dense material, the values of δ approach to 1.0 and are in close proximity with each other except for Lee and Kim [26]. The difference in the values of δ for Lee and Kim [26] with other researchers is remarkable. Further, it can be seen that for R greater than 0.80, δ is positive and the square of yield strength, Y, in Eq. (1) will be positive and does not violate the yield state of uniaxial and triaxial compression. Moreover, at the apparent relative density, R = 0.3, the δ is less than zero indicating that the loose powder have zero strength. Shima and Oyane [12] have all yield criterion parameters different from other researchers as presented in Table 3, however, their values for A and B are same with all other researchers as can be seen in Table 4, while the values for δ are in close range of Doraivelu et al. [18] and Park [25].

As explained above, the following yield criteria parameters are chosen to calculate the effective or equivalent stress in the PM materials as A = 2 + R², B = (1 − R²)/3, δ = 2R² − 1. Eq. (4) can now be written as

$$Y_0 = \sigma_{eff} = \left[\frac{(\sigma_z^2 + 2\sigma_\theta^2 - R^2(\sigma_\theta^2 + 2\sigma_\theta\sigma_z))}{2R^2 - 1}\right]^{0.5} \tag{5}$$

Mean stress under the assumption that $\sigma_\theta = \sigma_r$ for cylindrical coordinate system is:

$$\sigma_m = \frac{\sigma_r + \sigma_\theta + \sigma_z}{3} = \frac{2\sigma_\theta + \sigma_z}{3} \tag{6}$$

The stress formability factor (β) demonstrates the impact of hydrostatic and equivalent stress on the forming limit and can be expressed as [15]

$$\beta = \frac{3\sigma_m}{\sigma_{eff}} \tag{7}$$

The effective strain (ε_{eff}) in cylindrical axes [4] is expressed as:

$$\varepsilon_{eff} = [(2/(3(2 + R))][(\varepsilon_z - \varepsilon_\theta)^2 + (\varepsilon_\theta - \varepsilon_z)^2] + ((\varepsilon_z + 2\varepsilon_\theta)^2/3)(1 - R^2)]^{0.5} \tag{8}$$

where ε_θ = hoop strain and ε_z = axial strain and is given as:

$$\sigma_z = \frac{\text{load}}{\text{contact surface area}} \tag{9}$$

$$\varepsilon_z = \ln\left(\frac{h_f}{h_o}\right) \tag{10}$$

$$\varepsilon_\theta = \varepsilon_r = \ln\left(\frac{D_f}{D_o}\right) \tag{11}$$

where h_o = initial height; h_f = final height; D_o = initial diameter and D_f = final contact diameter.

Further, Ramesh et al. [2] considered the forged diameters in determining the hoop strain stated as below

$$\varepsilon_\theta = \ln\left[\frac{2D_b^2 + D_c^2}{3D_o^2}\right] \tag{12}$$

where D_b = final bulged diameter and D_c = final contact diameter.

Eq. (1) can be written using the Ludwik equation as:

$$AJ_2^{/} + BJ_1^2 = Y^2 = \delta(K\varepsilon_{eff}^n)^2 \tag{13}$$

where K = stress coefficient and n = hardening exponent. Eqs. (5) and (8) are used to evaluate the stress coefficient and the hardening exponent in the modified Ludwik equation for PM materials to evaluate the instantaneous stress coefficient (K_i) and instantaneous hardening exponent (n_i), where σ is effective stress and ε is equivalent strain. The derivation is as follows:

Taking successive stress on the compact as 1, 2, 3, ..., (j − 1) and j. Thus, the Ludwik equation gives:

$$\sigma_j = K\varepsilon_j^n \tag{14}$$

Table 3 – Yield criterion parameters.

Researcher	A	B	δ
Doraivelu et al. [18]	$2 + R^2$	$(1 - R^2)/3$	$2R^2 - 1$
Shima and Oyane [12]	$3/(1 + 0.6889(1 - R)^{1.028})$	$0.6889(1 - R)^{1.028}$	$R^5/(1 + 0.6889(1 - R)^{1.028})$
Park [25]	$2 + R^2$	$(1 - R^2)/3$	$1.44R^5/(2.44 - R)$
Lee and Kim [26]	$2 + R^2$	$(1 - R^2)/3$	$((R - R_c)/(1 - R_c))^2$

Table 4 – Relationship between the constant A, B and δ and the relative density.

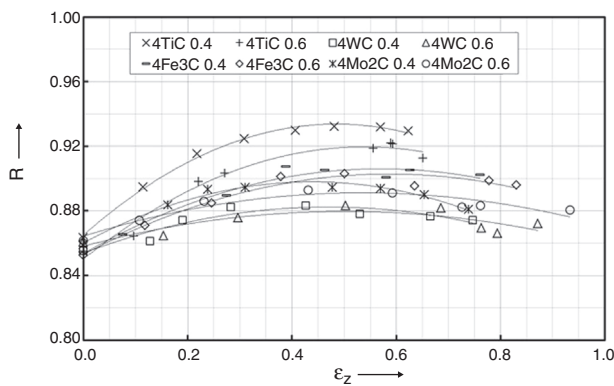| R	0.84			0.88			0.92			0.96			1		
Researcher	A	B	δ	A	B	δ	A	B	δ	A	B	δ	A	B	δ
Doraivelu et al. [18]	2.71	0.10	0.41	2.77	0.08	0.55	2.85	0.05	0.69	2.92	0.03	0.84	3	0	1
Shima and Oyane [12]	2.72	0.10	0.38	2.78	0.08	0.49	2.85	0.05	0.63	2.93	0.03	0.80	3	0	1
Park [25]	2.71	0.10	0.38	2.77	0.08	0.49	2.85	0.05	0.62	2.92	0.03	0.79	3	0	1
Lee and Kim [26]	2.71	0.10	0.04	2.77	0.08	0.16	2.85	0.05	0.36	2.92	0.03	0.64	3	0	1

Fig. 1 – Correlation between R and ε_z.

$$\sigma_{j-1} = K\varepsilon_{j-1}^n \tag{15}$$

Deducting Eqs. (14) and (15) gives

$$K_i = \frac{\sigma_j - \sigma_{j-1}}{\varepsilon_j^n - \varepsilon_{j-1}^n} \tag{16}$$

Now, dividing the Eq. (14) by Eq. (15) and taking the natural logarithm gives

$$n_i = \frac{\ln(\sigma_j/\sigma_{j-1})}{\ln(\varepsilon_j/\varepsilon_{j-1})} \tag{17}$$

Eqs. (16) and (17) are used to find the stress coefficient and hardening exponent, respectively.

3. Results and discussion

During the deformation of PM parts, it is known [26–30] that density is constantly improved due to induced strain. Fig. 1 gives the correlation of R and ε_z showing the densification characteristics of sintered aluminum composites for varying initial densities and different carbide reinforcement. The induced hydrostatic stress present in the preforms during the upsetting operation has a major part in pore elimination of PM parts and depends on friction, porosity, geometry

and respective compositions. The extent of densification is not the same for varying initial densities and different carbide reinforcement. Higher values of densification rate are observed for smaller initial density preforms. The reason for this is the higher requirements of hydrostatic force to close more number of pores found in the lower initial relative density compacts resulting in large amount of densification. The same can be verified from Fig. 2. Al-4TiC composite exhibited greater densification rate and greater final density followed by Al-4Fe$_3$C composite and then Al-4Mo$_2$C composite. Al-4WC composite showed the smallest densification rate and smallest final density attainment. Further, the densification rate during the final stages of deformation is notably lower when compared to the initial stage. During the forming practice the particles and pores stretch perpendicular to the load axis (Fig. 3). This provides more material resistance to deformation. The shapes of pores after sintering process are nearly spherical (Fig. 3a) while during the later stages of deformation it becomes almost cylindrical in shape (Fig. 3b).

Workability limit diagram is used as a reference to estimate the failure during metal forming and can be used effectively for PM forming as complex deformation mechanics is involved. The workability limit diagram shows the safe zone and failure zone in further processing of the PM products and can be used effective to understand when to activate re-pressing process on the free surface of PM part to avoid cracks and failure. This will help in the design of dies and process
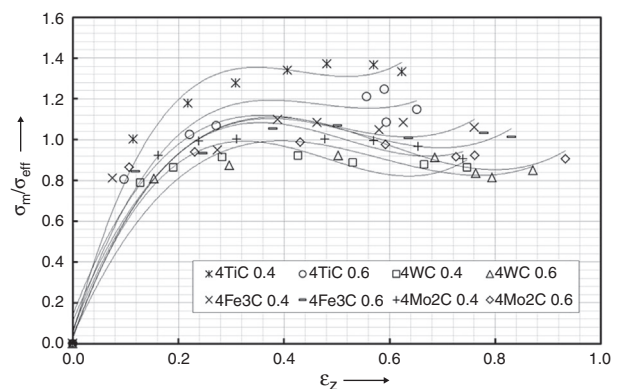

Fig. 2 – Correlation between σ_m/σ_{eff} and ε_z.
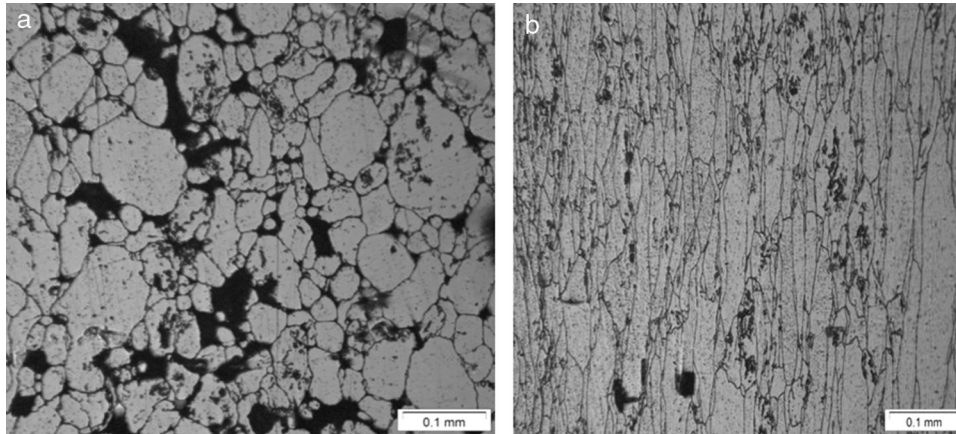
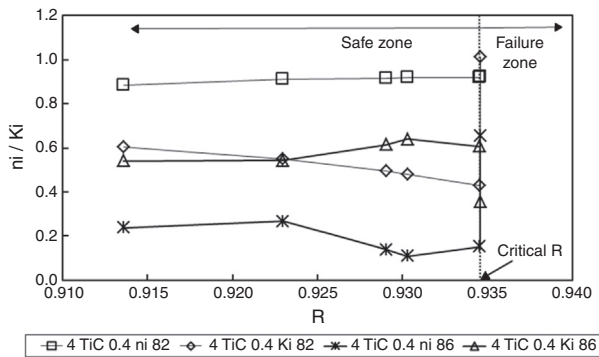**Fig. 3 – Micrographs of Al-4TiC at the edge of the specimen: (a) undeformed and (b) fully deformed.**

Fig. 4 – Workability limit diagram for PM Al4TiC composites.

operation for PM close die forging. Once the pores penetrate to the surface of the compact, it is difficult to repair the crack by re-pressing or other process and hence, this workability limit diagram is important in the forming of PM parts and in die design.

It is well understood that these two parameters, strain hardening exponent and stress coefficient, are important to study in the forming of MMC's. Several researchers have used these two parameters in the development of successful PM parts and procedures [4,31–33]. Further, Narayan et al. [34] introduced two new parameters called density hardening exponent and density strength coefficient to study the hardening phenomenon of sintered plain carbon steel preforms. Figs. 4–7 shows the workability limit diagram plotted using instantaneous ni and instantaneous Ki against relative density. The initial AR is chosen to be 0.4. The ni and Ki is calculated using the equations derived from the logarithmic graph of axial stress and strain as explained in detail in Section 2.3. At the start of deformation, the applied stress is significant in comparison to the axial deformation as to overcome the initial yield stress. Initially the applied stress is not adequate to collapse the large amount of pores and the stress values rise considerably for small amounts of densification and deformation resulting in higher ni values initially. This does not indicate strain hardening in the material and is always ignored

[34]. Hence, Figs. 4–7 are plotted for intermediate and final stages of deformation.

In all the plots the safe zone, failure zone and critical relative density are shown. The zones and critical relative density were determined by the changeover point on the slope of the linear line, which defines the minimum relative density of the sintered parts before existing pores may appear on the free surface of the parts causing the failure. Workability is the amount to which the material can be deformed before failure. In the final stages of deformation, the PM part nears full density with 5–8% porosity, which is hard to eliminate. The
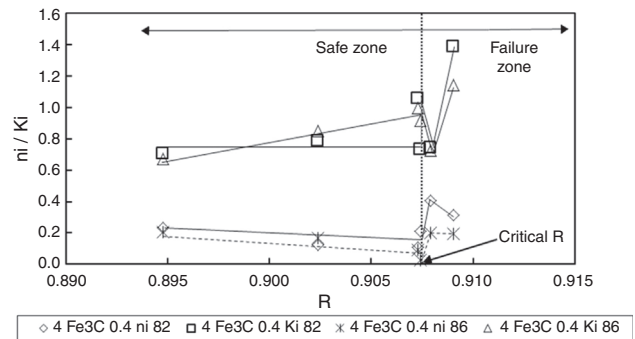

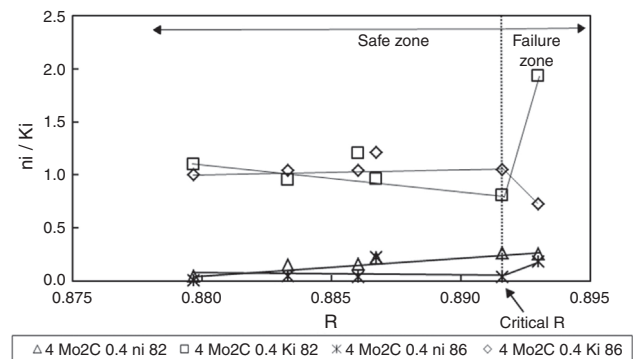**Fig. 5 – Workability limit diagram for PM Al4Fe$_3$C composites.**

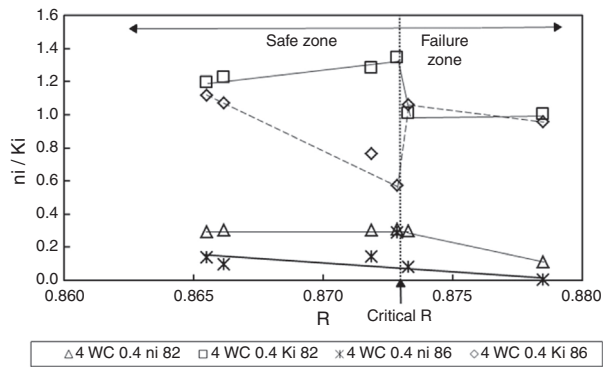**Fig. 6 – Workability limit diagram for PM Al4Mo$_2$C composites.**

Fig. 7 – Workability limit diagram for PM Al4WC composites.

PM parts are extremely strain hardened at this stage, hence, to further eliminate the residual pores require high load that considerably increases the strain hardening values and when these remaining pores collapse it considerably decreases the strain hardening values. This causes the instabilities in the ni and Ki values during the final stages of deformation. The same is also presented in Refs. [34,35]. These fluctuations in the ni and Ki values during the last stage of forming is a sign of failure if deformation is not stopped or if re-pressing on the free surface in close die forging is not employed. The critical density can be used in die design and to produce defect free parts. For any axial strain, the hydrostatic stress is higher for Al-4TiC composites, followed by Al-4Fe$_3$C, Al-4Mo$_2$C and smallest for Al-4WC composites as seen in Fig. 2. This means Al-4WC preforms has room for further deformation as long as it has no visible cracks on the free surface. The workability diagram of Al4WC (Fig. 7) can be effectively utilized here for this purpose.

In Figs. 4–7 the critical relative density is found to be 93.5%, 90.8%, 89.2% and 87.3% for PM Al4TiC, Al4Fe$_3$C, Al4Mo$_2$C and Al4WC, respectively. These critical relative densities give the workability of the respective materials to produce defect free parts. Once the respective critical relative density is reached during deformation the chances of cracks appearing is high and hence deformation needs to stop or repressing needs to be employed to produce healthy PM aforementioned parts. It is noted that the critical relative density is highest for TiC reinforced aluminum, followed by Al-4Fe$_3$C composite and
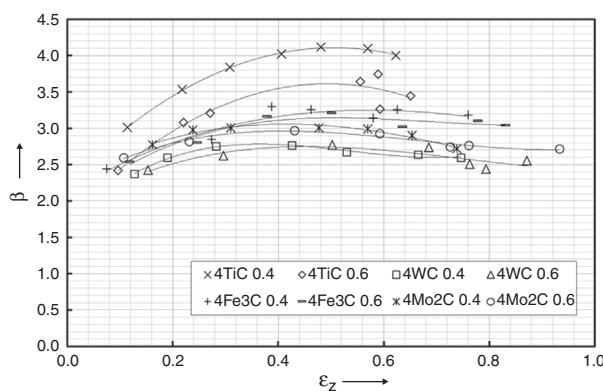
then Al-4Mo$_2$C composite. Al-4WC composite had the smallest critical relative density. One of the reasons for this is that the formability of TiC reinforced aluminum composites was found to be higher followed by Fe3C and Mo2C reinforced aluminum composites. WC reinforced aluminum composites gave the smallest formability stress index against axial strain (Fig. 8). Further, the composites are designed by weight ratio and titanium carbide particles had the lowest weight followed by iron carbide, molybdenum carbide and then tungsten carbide (Table 2). Hence, the amount of smaller and fine pores existing in Al-4TiC compact is higher compared to other materials tested here and hence, for the same reason the critical relative density is higher for TiC composite in comparison with other composites.

4.   Conclusion

The workability behavior of Al-4TiC, Al-4WC, Al-4Fe$_3$C and Al-4Mo$_2$C are analyzed and the finding are as follows:

- The amount of densification is higher in TiC reinforced aluminum followed by Fe$_3$C, then Mo$_2$C and lowest for WC reinforced aluminum composites. Further, smaller aspect ratio composites gave good densification rate than bigger aspect ratio composites. Higher values of densification rate are observed for smaller initial relative density preforms. This ensured better formability behavior for TiC reinforced aluminum compacts and smaller AR compacts. The accompanying compressive hydrostatic stress is responsible for densification.
- The particles and porosity deform and elongate perpendicular to the direction of load application.
- The instantaneous strain hardening exponent and instantaneous stress coefficient are utilized to plot the forming limit diagrams highlighting the safe working zones. These plots can be effectively used in the design of forming operations for the aforementioned composites.
- The critical relative density is found to be 93.5%, 90.8%, 89.2% and 87.3% for PM Al4TiC, Al4Fe$_3$C, Al4Mo$_2$C and Al4WC, respectively. The safe working zone is found to be the narrowest for Al4WC.

Conflicts of interest

The authors declare no conflicts of interest.

R E F E R E N C E S

Fig. 8 – Correlation between β and ε_z.

[1] Zhang XQ, Peng YH, Li MQ, Wu SC, Ruan XY. Study of workability limits of porous materials under different upsetting conditions by compressible rigid plastic finite element method. J Mater Eng Perform 2009;9:164–9.
[2] Ramesh B, Senthivelan T. Formability characteristics of aluminium based composite – a review. Int J Eng Technol 2010;2:1–6.
[3] Rahman MA, El-Sheikh MN. Workability in forging of powder metallurgy compacts. J Mater Process Technol 1995;54:97–102.

[4] Narayanasamy R, Ramesh T, Pandey KS. An investigation on instantaneous strain hardening behaviour in three dimensions of aluminium–iron composites during cold upsetting. Mater Sci Eng A 2005;391:418–26.

[5] Spigarelli S, Cerri E, Cavaliere P, Evangelista E. An analysis of hot formability of the 6061 + 20% Al_2O_3 composite by means of different stability criteria. Mater Sci Eng A 2002;327:144–54.

[6] Rahimian M, Ehsani N, Parvin N, Baharvandi H. The effect of particle size, sintering temperature and sintering time on the properties of Al–Al2O3 composites, made by powder metallurgy. J Mater Process Technol 2009;209:5387–93.

[7] Danninger H, Jangg G, Weiss B, Stickler R. Microstructure and mechanical properties of sintered iron – Part I: Basic consideration and review of literature. Powder Metal Int 1993;25:170–3.

[8] Kuhn HA, Downey CL. How flow and fracture affect design of preforms for powder forging. Int J Powder Metal Powder Technol 1974;10:59–66.

[9] Hwang BB, Kobayashi S. Deformation characterization of powdered metals in compaction. Int J Machine Tools Manuf 1990;30:309–23.

[10] Bao Y. Dependence of ductile crack formation in tensile test on stress triaxiality, stress and strain ratios. Eng Fract Mech 2005;72:505–22.

[11] Bao Y, Wierzbicki T. On fracture locus in the equivalent strain and stress triaxiality space. J Eng Mater Technol 2004;46:81–98.

[12] Shima S, Oyane M. Plasticity theory for porous metals. Int J Mech Sci 1976;18:285–91.

[13] Green RJ. A plasticity theory for porous solids. Int J Mech Sci 1972;14:215–24.

[14] Narayanasamy R, Senthilkumar V, Pandey KS. Effect of titanium carbide particle addition on the densification behaviour of sintered P/M high strength steel preforms during cold upset forming. Mater Sci Eng A 2007;456:180–8.

[15] Narayanasamy R, Ponalagusamy R, Subramanian KR. Generalized yield criteria of porous sintered powder metallurgy metals. J Mater Process Technol 2001;110:182–5.

[16] Narayanasamy R, Anandakrishnan V, Pandey KS. Effect of geometric work-hardening and matrix work-hardening on workability and densification of aluminium–3.5% alumina composite during cold upsetting. Mater Des 2008;29:1582–99.

[17] Vujovic V, Shabaik AH. A new workability criterion for ductile materials. J Eng Mater Technol 1986;108:245–9.

[18] Doraivelu SM, Gegel HL, Gunasekara JS, Malas JC, Morgan JT. A new yield function for compressible P/M materials. Int J Mech Sci 1984;26:527–35.

[19] Ko BC, Park GS, Yoo YC. The effects of SiC particle volume fraction on the microstructure and hot workability of SiCp/AA 2024 composite. J Mater Process Technol 1999;95:210–5.

[20] Luo J, Li M, Yu W, Li H. The variation of strain rate sensitivity exponent and strain hardening exponent in isothermal compression of Ti–6Al–4V alloy. Mater Des 2010;31:741–8.

[21] Rajeshkannan A, Narayan S. Strain hardening behaviour in sintered Fe–0.8%C–1.0%Si–0.8%Cu powder metallurgy preform during cold upsetting. J Eng Manuf 2009;223:1567–74.

[22] Rajeshkannan A, Narayan S. Phenomenon of instantaneous work hardening characteristics of sintered cold deformed Cu alloy preforms. Adv Mater Res 2013;651:295–301.

[23] Derakhshandeh RH, Jahromi AJ. An investigation on the capability of equal channel angular pressing for consolidation of aluminium and aluminium composite powder. Mater Des 2011;32:3377–88.

[24] Sahin Y. Preparation and some properties of SiC particle reinforced aluminium alloy composites. Mater Des 2003;24:671–9.

[25] Park JJ. Constitutive relations to predict plastic deformations of porous metals in compaction. Int J Mech Sci 1995;37:709–19.

[26] Narayanasamy R, Selvakumar N. Deformation behaviour of cold upset forming of sintered Al–Fe composite preforms. J Eng Mater Technol 2005;127:251–6.

[27] Rajeshkannan A, Pandey KS, Shanmugam S, Narayanasamy R. Sintered Fe–0.8%C–1.0%Si–0.4%Cu P/M preform behaviour during cold upsetting. J Iron Steel Res Int 2008;15:92–7.

[28] Kuhn HA, Lawley A. Powder metallurgy processing. New York: Academic Press; 1978. p. 99–138.

[29] Rajeshkannan A, Pandey KS, Shanmugam S. Some investigation on the cold deformation behaviour of sintered iron–0.8% carbon alloy powder preforms. J Mater Process Technol 2008;203:542–7.

[30] Lewis RW, Khoei AR. A plasticity model for metal powder forming processes. Int J Plast 2001;17:1659–92.

[31] Selvakumar N, Narayanasamy R. Phenomenon of strain hardening behaviour of sintered aluminium preforms during cold axial forming. J Mater Process Technol 2003;142:347–54.

[32] Straffelini G. Strain hardening behaviour of powder metallurgy alloys. Powder Metal 2005;48:189–92.

[33] Ni DR, Chen DL, Wang D, Xiao BL, Ma ZY. Tensile properties and strain-hardening behaviour of friction stir welded SiCp/AA2009 composite joints. Mater Sci Eng A 2014;608:1–10.

[34] Narayan S, Rajeshkannan A. Influence of carbon content on strain hardening behaviour of sintered plain carbon steel preforms. J Iron Steel Res Int 2011;18:33–40.

[35] Rajeshkannan A, Pandey KS, Shanmugam S, Narayanasamy R. Deformation behaviour of sintered high carbon alloy powder metallurgy steel in powder preform forging. Mater Des 2008;29:1862–7.